Instantaneous Lift and Motion Characteristics of Butterflies in Free Flight

Madhu K. Sridhar[1], Chang-kwon Kang[2], and David B. Landrum[3]
University of Alabama in Huntsville, Huntsville, AL 35899

Monarch butterflies stand out among insects with the longest insect migration distance, up to 4,000 km. In order to understand the intriguing aerodynamic performance of Monarch butterflies, an optical tracking facility is used to record the flapping wing motion, body motion, and resultant lift. The system automatically tracks reflective markers, which are modified to reduce the effects of additional mass on the flight characteristics. Position and Euler angles of the thorax, the abdomen, and the right forewing of a freely flying Monarch are determined as a function of time. Analysis of a single representative flight suggests that the position, orientation, and shape of the body and wings continuously vary during the flight. Instantaneous lift, determined based on the force balance, suggests that the butterfly in climbing flight gains most of the lift during the downstroke, with a peak of six times its weight, resulting in a climb rate of 1.1 m/s, where the thorax and abdomen are aligned. During the upstroke, the lift is negative with a much lower magnitude yielding a lower climb rate of around 0.5 m/s. At the end of this lower climb regime, the relative angle between the thorax and the abdomen is the largest. We believe our experimental study can help improve our understanding of biological flight and development of micro flapping robots.

Nomenclature

a_z	=	acceleration in the vertical direction	[m/s^2]
AR	=	wing aspect ratio	[1]
A_1, A_2	=	abdomen markers	[1]
c	=	chord	[m]
C_L	=	lift coefficient	[1]
f	=	flapping frequency	[Hz]
F_z	=	force in the vertical direction	[N]
g	=	acceleration due to gravity	[m/s^2]
l_a	=	abdomen marker separation length	[m]
l_t	=	thorax marker separation length	[m]
L	=	lift	[N]
LW_1, LW_2, LW_3, LW_4	=	left forewing markers	[1]
L_a	=	length of abdomen	[m]
L_h	=	length of head	[m]
L_t	=	length of thorax	[m]
m	=	butterfly mass	[kg]
$\mathbf{r}_{centroid}^{t}$	=	position vector of the centroid at time t	[m]
$\mathbf{r}_{centroid}^{t0}$	=	position vector of the centroid at reference time t_0	[m]
$\mathbf{r}_{trans}$	=	translation vector, $\mathbf{r}_{trans} = \mathbf{r}_{centroid}^{t} - \mathbf{r}_{centroid}^{t0}$	[m]
$\mathbf{r}_{T1}$, $\mathbf{r}_{T2}$, $\mathbf{r}_{LW3}$ $\mathbf{r}_{RW3}$	=	position vector of markers T_1, T_2, LW_3 and RW_3	[m]
$\mathbf{r}_{T1,I}$	=	position vector of marker T_1 in inertial frame	[m]
$\mathbf{r}_{T1,b}$	=	position vector of marker T_1 in body frame	[m]
R	=	half wing span	[m]

---

[1] Graduate Student, Mechanical and Aerospace Engineering, Technology Hall C200, AIAA Student Member
[2] Assistant Professor, Mechanical and Aerospace Engineering, Technology Hall N266, AIAA Senior Member
[3] Associate Professor, Mechanical and Aerospace Engineering, Technology Hall N267, AIAA Associate Fellow

RW$_1$, RW$_2$, RW$_3$, RW$_4$	=	right forewing markers	[1]
R$_{I \to b}$	=	rotation matrix from inertial frame to body frame	[1]
R$_{b \to w}$	=	rotation matrix from body frame to wing frame	[1]
S	=	wing area	[m^2]
T$_1$, T$_2$, T$_3$	=	thorax markers	[1]
V_x, V_y, V_z	=	x-, y- and z- components of body velocity	[m/s]
V	=	body velocity	[m/s]
W_b	=	body weight	[N]
X_I, Y_I, Z_I	=	coordinate axes of inertial reference frame	[m]
X_V, Y_V, Z_V	=	coordinate axes of velocity vector adjusted inertial reference frame	[m]
x_b, y_b, z_b	=	coordinate axes of body reference frame	[m]
α	=	feathering angle	[deg]
β	=	stroke plane angle	[deg]
γ	=	flapping angle	[deg]
δ	=	deviation angle	[deg]
ϕ	=	body roll angle	[deg]
ψ_T	=	body yaw angle	[deg]
ψ_V	=	yaw angle of body velocity vector projection	[deg]
ρ	=	air density	[kg/m^3]
θ	=	thorax pitch angle	[deg]
χ	=	abdomen angle with horizontal	[deg]
ζ	=	positional angle	[deg]
Z	=	stroke amplitude	[deg]

I.   Introduction

INSECT flight has garnered a lot of attention from both the engineering and biology communities in the recent decades, often driven by an interest in bioinspired or bio-mimicked design of small unmanned aerial vehicles, called Micro-air vehicles (MAVs). MAVs are classified as miniature aerial vehicles with wingspans less than 15cm[1]. Given their small size compared to conventional drones, MAVs have even more potential to revolutionize our sensing and information gathering capabilities in areas such as environmental monitoring and homeland security[1]. There are two key challenges in MAV development that need to be addressed: i) their power efficiency and ii) stability in an unsteady flight environment[2]. State-of-the-art MAVs, e.g. the Nano Hummingbird[3], DelFly[4], or Harvard's robotic fly[5] have limited onboard power sources due to their small sizes. Even larger commercially available drones can only fly 10 to 25 minutes on the onboard battery. Moreover, the flight environment is often unsteady with wind gusts of magnitudes that are the same as their operating speeds.

Biological flyers showcase desirable flight characteristics and performance in rapid maneuvers[1] that can guide the design of MAVs. These flapping flyers utilize wing kinematics, deformable wing shapes, and large scale vortical structures to enhance lift and thrust[6]. For decades, the aerodynamics of insect flight remained inexplicable. A well-known example is the myth that bumblebees cannot fly according to the classical, aerodynamics theories[7]. Since then, many findings on unsteady lift enhancing mechanisms, such as the clap and fling[8], dynamic stall via leading-edge vortices[9], wake-capture[10,11], and rotational forces due to combined translation and rotation[10,12], have enhanced our understanding of how insects stay aloft[6]. These unsteady physical processes are particularly important for small flyers, such as insects, which operate at low Reynolds number of around $O(10^2)$ to $O(10^3)$. In low Reynolds number regimes, both viscous, inertial, and unsteady effects are important. Furthermore, the aerodynamic efficiency is reduced significantly for stationary non-flapping flight at lower Reynolds numbers, compared to that of passenger airplanes[6,13].

Butterflies are also known to use clap and peel, a variant of clap and fling, wake-capture, leading-edge vortex, and rotational mechanisms[14]. However, compared to the wealth of research on the aerodynamics of biological flyers such as flies[10,15], bees[16,17], dragonflies[18–22], as well as birds and bats[6], the flight of butterflies remains inadequately understood due to their many unique characteristics. They are extremely evasive with agile maneuvers[23–26] and large body undulations with closely coupled wing-body interaction[25,27]. Biologists have conjectured that butterflies became evasive to escape from predators, such as birds[28–30]. Among these flapping flyers, the Monarch butterfly, *Danaus plexippus*, stands out with the longest migration distance among insects - up to 4,000 km over the course of

three months[31–33]. They fly from eastern North America to central Mexico during the fall[34,35]. Glider pilots have spotted migrating Monarch butterflies at an altitude of 1,250 m[36]. At these high altitudes, the Monarch can take advantage of favorable weather and wind patterns in the boundary layer of the earth[31,37,38], presumably to conserve energy[39,40]. They use magnetic and sun compasses for navigation to Mexico[41]. Their long migration suggests that they are extremely efficient flyers. Moreover, they flap, glide[29], and perform agile maneuvers while climbing up and down with ease[23].

However, even though the morphological characteristics of the Monarch butterflies are well studied[42,43], the structural and aerodynamic mechanisms behind their intriguing maneuverability has not been elucidated. Also, butterfly wing area is relatively large with fore and hindwings that flap in sync[44], unlike dragonflies with relatively long wings often flapping out of sync[20,21]. Furthermore, there are limited experimental results that characterize the aerodynamics of their large flexible wings with complex vein structures[45–47].

Many insect motion measurements consider tethered flight[18] or hovering flight[8,18,42]. However, measurements of tethered insects may not represent the actual motion in free flight[48]. The main difficulty faced in recording kinematic data of a forward flying insect is that it must fly through a relatively small volume that is in full view of the cameras. Many studies have used wind tunnels[26,42,48] or 2D image processing[45]. 3D photogrammetric methods[27,49–52] were also used that capture the three-dimensional wing shape deformation of dragonfly wings[53], however these measurements are still limited to a relatively small capture volume.

In our earlier work, we used twenty two high speed motion tracking cameras in a capture volume of 5.7 m×9.1 m×3.0 m to measure and report the flapping wing angle and body trajectory of freely flying Monarch butterflies[54]. In this capture volume butterflies can fly unobstructed for a large sequence of flaps without requiring any extra equipment to entice flight. The number of high resolution cameras and the post processing software provide a unique opportunity to continuously record flights and accurately process entire flights in minutes so that a vast amount of data can be collected and compared to previous experiments. We showed that the wing beat frequency was similar to the undulating motion of the body, suggesting that the flapping wing aerodynamics and flight dynamics are closely coupled to each other. Moreover, the butterfly wings significantly deform during flight. An accurate measurement of both wing kinematics and the body motion is crucial to understand the dynamic flight stability and control of a flapping insect[55].
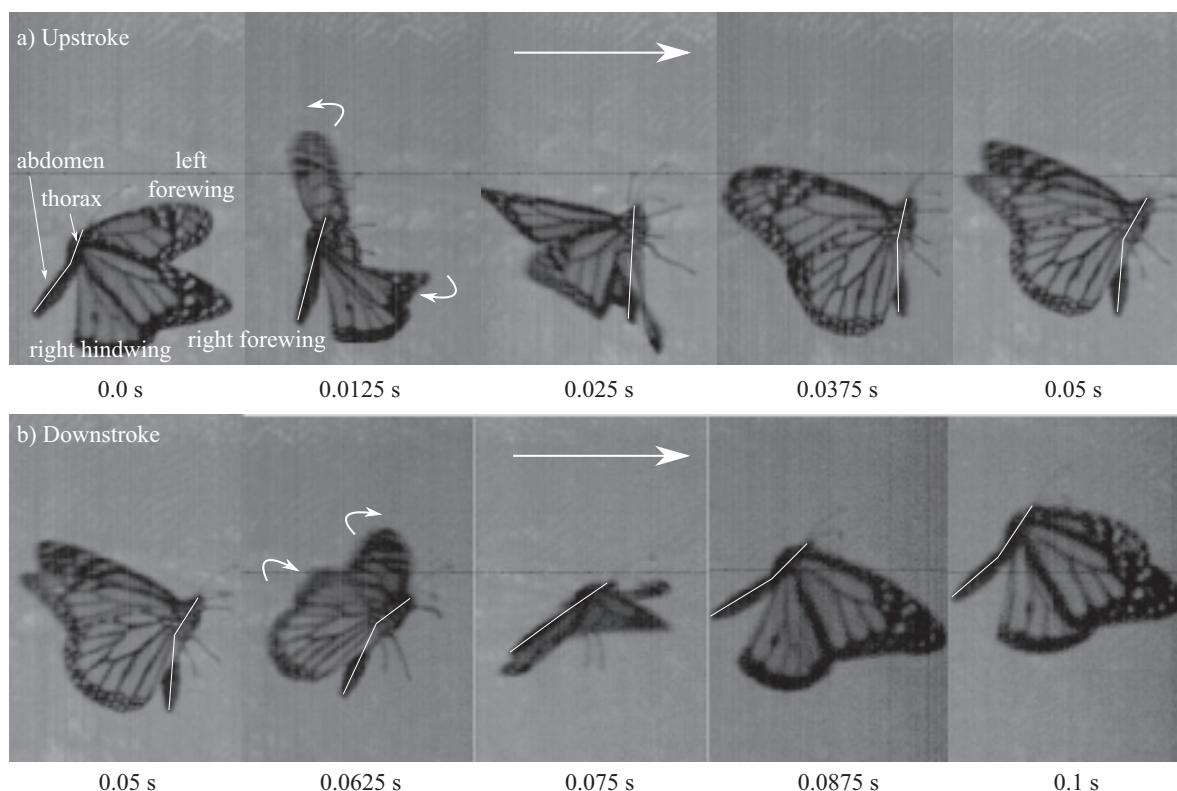

Figure 1. High speed camera snapshots of a free flying Monarch butterfly. Body rotation and wing motions continuously vary during the transition from a forward to a climbing flight. (a) Upstroke; (b) Downstroke.

American Institute of Aeronautics and Astronautics

For insects, with a notable exception of butterflies, the instantaneous information from flapping may not be as critical for simple flight dynamics models because flapping time is much faster than that of the entire flyer[6,56]. However, Lin et al.[27] showed that moment of inertia of the body plays a significant role in maneuverability of the painted lady butterflies, implying that a time-averaged analysis may not be ideal in the analysis of butterfly flight. Moreover, the orientation and the shape of the butterfly body continuously change during flight[57]. Sunada et al.[58] showed that the moment generated by the body rotation caused the stroke plane orientation to change during flight, affecting the aerodynamics of the flapping wings. More recently, Fei and Yang[59] carried out computational simulations of free flying butterflies by prescribing body angles and suggested that the butterfly adjusts its body orientation to minimize the drag force. However, their body angle was prescribed and the effects of the abdominal motion were left for future exploration.

The relative motion of the abdomen with respect to the thorax within a flapping cycle as shown in Figure 1 introduces additional complexity in analyzing the coupled wing-body motion. Monarch butterfly, as captured by our high speed camera system, continuously vary their relative angle between the thorax and abdomen, its thorax orientation with respect to the horizontal, and wing shape and orientation during a flight in a closely coupled manner. However, simultaneous quantification of the position and orientation of these different body parts and wings have not been reported before. Moreover, the aerodynamic and flight dynamic influence of a continuously rotating and deforming body on the butterfly flight and its coupled interaction with the flapping motion of the wings is not fully reported and understood.

The objective of this paper is three-fold. Firstly, we resolve the overall body orientation into two main segments: the thorax and abdomen. In our previous study[54], we reported the undulating motion of the body by tracking one marker placed on the thorax. In the current study, we provide a more detailed representation of the body by recording the thorax and the abdomen orientations separately. Secondly, we determine the instantaneous lift coefficient during climbing flight by considering a force balance. Thirdly, the state of the body during free flight is considered as a six degree-of-freedom representation including the three Euler angles. The flapping motion of the forewing is also represented as a six degree of freedom (DOF) system. We also report on the orientation of the stroke plane, consistent with the definition by Ellington[60]. We consider a single representative flight and quantify the body orientation and the wing angles during two flapping cycles. We collected 19 test flights using the above framework and a statistically relevant analysis will be reported in the future.

The organization of the paper is as follows. First, we provide a detailed description of the experimental methodology in Section II. This is followed by the discussion of results from a single flight test with a focus on body and wing kinematics in Section III. Finally, we analyze and discuss the 6-DOF representation of the body and wing as well as the force balance on the resulting trajectory of a freely flying Monarch.

II. Methodology

A. VICON Motion Capture System

The experiments are conducted in the Autonomous Tracking and Optical Measurements (ATOM) laboratory at the University of Alabama in Huntsville (UAH). The ATOM lab is a motion capture facility which uses 33 VICON T40s cameras, Mx Giganet connectivity node, and Nexus[61] software, designed to track reflective markers in three-dimensional space. Maximum capture volume dimensions are 17.2 m × 9.1 m × 3.0 m. In our previous work[54], twenty two cameras were placed inside a smaller capture volume of 5.7 m × 9.1 m × 3.0 m to increase the number of cameras in the capture volume. The relatively large size of the capture volume with respect to the size of a butterfly enables data capture with unrestricted free flight trajectories.

The VICON T40s cameras record at 515 fps at a full resolution of 4 megapixels. They are equipped with a near infrared (NIR) strobe, and visible light filters to allow for operation under a variety of lighting conditions. The cameras track reflective markers specifically designed for motion capture systems and efficiently reflect the NIR light. Each camera contains an onboard processor which locates all markers recorded in a frame, calculates a circle fit and determines the centroid of the circle. The location of the centroid and radius are the only data that are sent to the Mx Giganet during a motion capture test. The Mx Giganet calculates the three-dimensional position of all markers seen by two or more cameras simultaneously and sends it to the VICON workstation and into Nexus. Depending upon the user's requirements, the data can be transmitted to the monitor for real time monitoring, or recorded for post processing. The output environment is the virtual work space, which provides a three-dimensional representation of the location of all cameras and position of the markers detected.

American Institute of Aeronautics and Astronautics

The motion capture system requires regular calibration, which is done before data is collected in the form of a dynamic calibration. Calibration requires the use of a T-shaped tool provided by VICON. The calibration tool has five markers with precise spacing, which are recognized by each camera. During calibration, the calibration tool is waved around the capture volume. As two or more cameras see all five markers on the tool simultaneously, the Giganet compares the images from the cameras to the known dimensions of the wand. The position of each camera can then be calculated from this information. This process happens over one thousand times during a single calibration. The system can then record data using the same calibration until vibrations in the walls or slippage in the cameras causes a loss in resolution of the data. It was found that a calibration at the beginning of each day of testing was sufficient to retain uniform resolution.
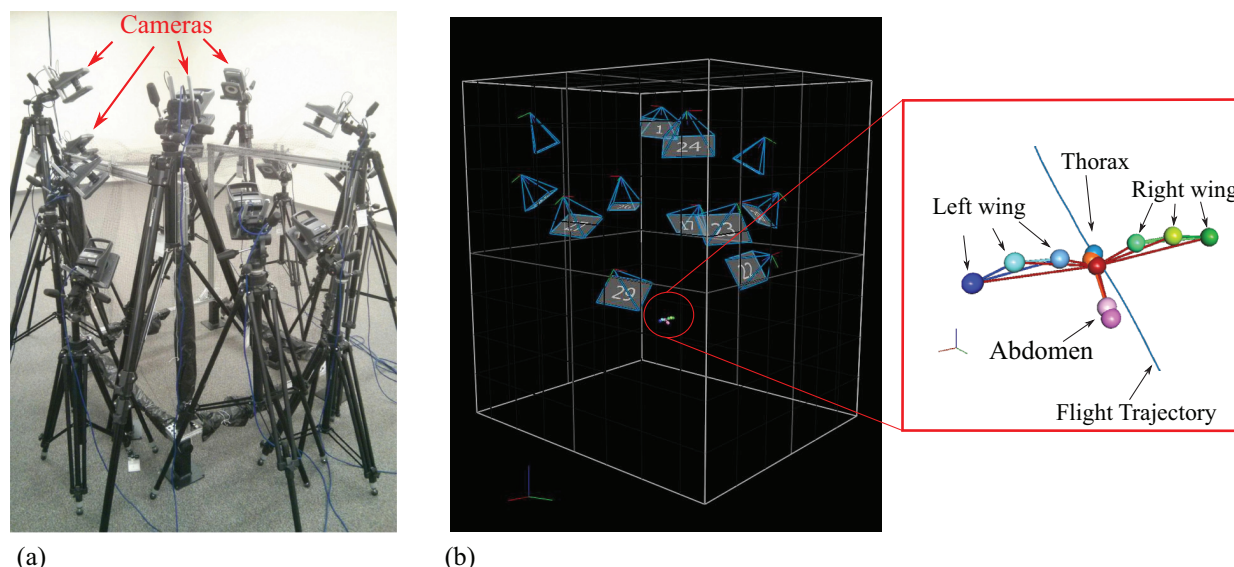

(a)   (b)

Figure 2. Experimental setup. (a) Physical capture volume. (b) Virtual capture volume and the camera positions as seen in Nexus with close up view of the reconstructed markers on the butterfly.

The motion capture system detects the three-dimensional position of reflective markers. We tested various markers sizes and shapes in our previous study[54]. A reflective rectangular tape of 3 mm size was chosen for its significantly reduced mass. This choice was critical to reduce the changes in flight behavior that could be caused by the addition of mass to the butterfly. Although the 3 mm markers are lighter, they are not well suited for placement on the body. The width of the thorax is of the order of 5 mm and a single 3 mm marker covers more than half of the thorax width. Additionally, to isolate thorax and abdomen motion, more than one marker is needed on the body. To meet this requirement, we reduced the size of the marker further down to a circular shape with diameter of 1.8 mm. To track these smaller markers, the distance between the camera and the marker had to be reduced. The capture volume was shrunk to 1.2 m × 1.2 m × 1.5 m with 12 VICON cameras (Figure 2) without affecting the tracking quality. The markers were cut using a hole punch which enabled us to standardize the marker shape and mass. A Python script was generated to post-process the recorded data from the motion capture system.

B. Monarch Butterflies and Testing Procedure

Monarch butterfly body can be divided into head, thorax and the abdomen regions. Head is at the forefront of the body which houses a pair of eyes and antennae. Thorax is located behind the head and the fore and hindwings extend from the thorax. The third region of the body is called the abdomen, which is a flexible, segmented and slender region. A snapshot of the body orientation during flight is shown in Figure 3(a). The length of the head, thorax and abdomen are denoted by L_h, L_t and L_a respectively. The thorax of a Monarch butterfly is a relatively rigid structure when compared to the abdomen. The thorax and the abdomen sections normally are not aligned in a straight line (Figure 1). Instead, the abdomen is positioned around a hinge point with respect to the thorax and is free to move up and down or laterally. Morphological data for five butterfly specimens measured before the testing is given in Table 1. The wing mass when compared to the corresponding body mass measured for two specimens were around 20%.

American Institute of Aeronautics and Astronautics

The Monarch butterflies are shipped in individual boxes packed in a Styrofoam cooler with ice packs to ensure the butterflies were kept safe through the shipping process. Monarch butterflies use cool temperatures during overwintering to reduce usage of their lipid reserves[62] which consequently reduces body activity and even impairs their ability to fly[32]. This state of reduced activity was used by the research team to more safely handle, measure and place markers on the specimens. During a week of testing, the first day consisted of removing each butterfly from the shipping container where they were kept chilled. The butterflies were kept cold as they were first weighed, markers were placed and were weighed again. The butterflies were then placed in terrariums under a directed incandescent lamp and allowed to rest overnight to attempt to reduce the potential effects of stress from handling and the addition of markers.

Table 1. Morphological data measured for five specimens. Current study corresponds to butterfly No. 1.

No.	Gender	Mass, m [g]	Half wingspan, R [mm]	Body width [mm]	Body length [mm]			Wing area, S [$\times10^{-4}$ m^2]	Wing loading [N/m^2]	Aspect Ratio, AR
					L_h	L_t	L_a			
1	M	0.458	48.94	5.93	4.9	9.3	19.5	27.895	1.612	3.863
2	M	0.443	49.04	5.68	4.3	8.7	19.1	26.069	1.667	3.820
3	M	0.477	48.60	6.01	4.4	8.6	21.2	25.057	1.867	3.839
4	F	0.361	47.51	5.04	3.8	9.3	18.0	26.695	1.326	3.756
5	M	0.402	49.92	5.85	3.7	8.9	20.1	24.529	1.679	3.790
Avg.		0.428	48.80	5.70	4.2	8.9	19.5	26.049	1.630	3.813

(a)   (b)
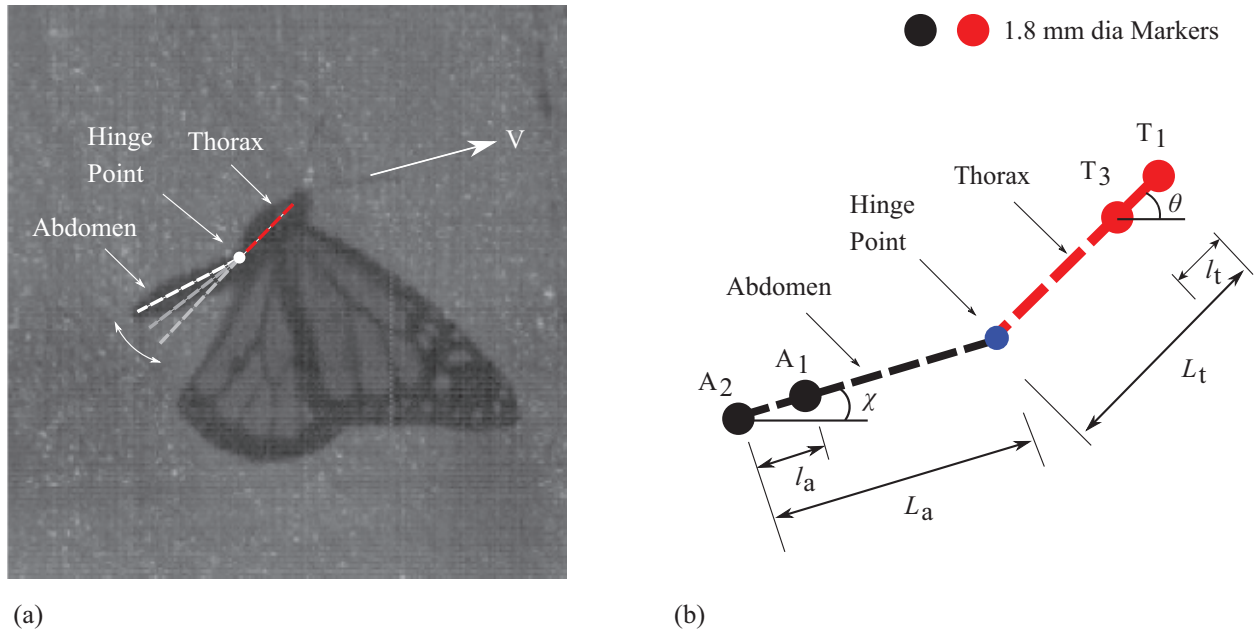
Figure 3. (a) A snapshot of a free flying Monarch butterfly at the end of downstroke with an elevated abdomen position. Abdomen can change its orientation with respect to the thorax during flight as indicated by dotted lines. (b) Definition of the thorax and the abdomen angles along with morphological definitions used in the current study.

C. Marker configuration

VICON motion capture system detects position of reflective markers. The sampling rate in this study was 200 Hz, double the rate in our previous work[54]. Markers are placed at strategic locations on the body and the wings of butterfly as shown in Figure 4(a). Three circular markers with a diameter of 1.8 mm, denoted as T_1, T_2 and T_3 are

American Institute of Aeronautics and Astronautics

placed on the thorax. Markers T_1 and T_3 are carefully aligned with the longitudinal axis of the body with a separation distance l_t=6.9 mm. A third marker T_2 is placed at a small offset of 2.6 mm to the left of the longitudinal axis. The thorax orientation is denoted by the line segment joining the markers T_1 and T_3. Similarly, markers A_1 and A_2 are placed longitudinally on the lower end of the abdomen at a separation distance l_a=3.9 mm. The abdomen orientation is denoted by the line segment between A_1 and A_2. The orientation of the thorax and the abdomen with respect to the horizontal are denoted by the angles θ and χ respectively (Figure 3(b)).

The wing markers are rectangular in shape with dimension of 2×3 mm. Markers RW_1, RW_2, RW_3 are placed on the leading edge of the right forewing at 0.4R, 0.7R and 1.0R respectively, where R=48.94 mm is the half wing span measured from the wing root. A fourth marker, RW_4, is placed on the trailing edge of the right forewing at 0.7R. The vector between RW_2 and RW_4 represents the chord of the right forewing at approximately 0.7R measured at $c_{0.7R}$=18.9 mm. On the leading edge of the left forewing, three markers LW_1, LW_2, and LW_3 are placed at 0.4R, 0.7R and 1.0R respectively. To prevent marker occlusion during the upstroke when the wings fold backwards, rectangular markers of 2×3 mm were placed on the underside of the wings at the same position as on the upper side of the wing.

Table 2. Reflective markers used in this study.

Marker Type	Usage	# of Markers	Total Marker Mass (g)	% Butterfly mass (0.458 g)	% Total wing mass (4 wings) (0.046 g)
1.8 mm dia. round	Thorax	3	0.0003	0.065	0.6
	Abdomen	2	0.0002	0.043	0.4
2×3 mm rectangle	Left Forewing	6	0.0083	1.82	16.6
	Right Forewing	8	0.0115	2.51	23
	Right Hindwing	2	0.0022	0.48	4.8
Total		19	0.0225	4.91	48.9

The placement of reflective tape markers on the body and wings add to the total mass of the butterfly. Reduction in the marker size and mass was achieved by improved calibration techniques. The smallest markers used in the current study were circular markers with a diameter of 1.8 mm. The mass of each of these markers were measured to be 0.063% of the total mass of the butterfly. The rectangular, 2×3 mm marker, with a larger marker area, which were required to track the rapid motion of the wings, weighed around 0.3% of the butterfly mass. The individual contribution from each marker is summarized in Table 2. The total marker mass remains under 5% of the total butterfly mass. Eight rectangular markers on the right forewing combine to about 23% of the total wing mass. We will report on the effects of number of wing markers on the resulting butterfly flight more in detail in the future.
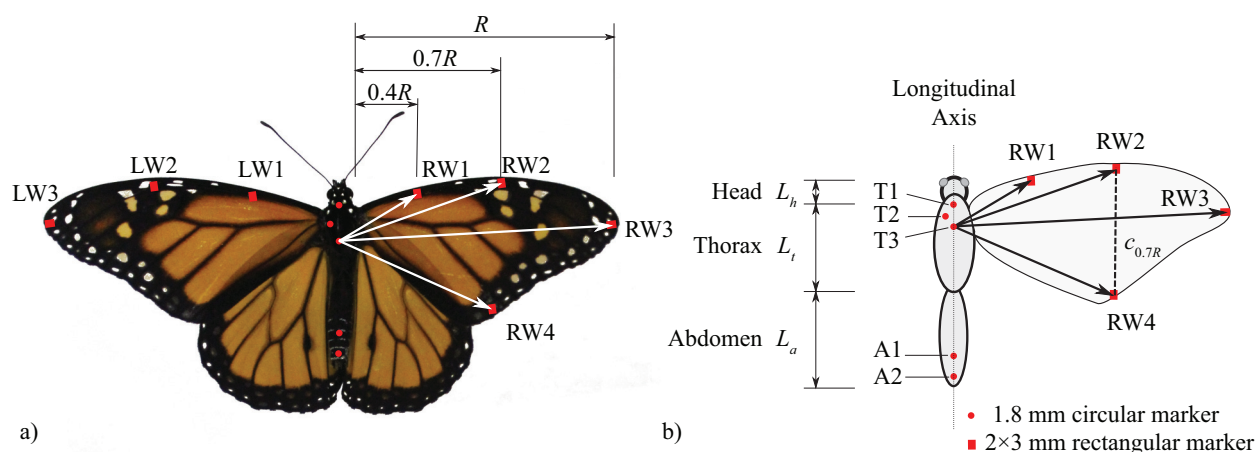

Figure 4. (a) Marker locations on the body and the wings of a Monarch specimen. (b) A schematic showing the marker labels and body morphology.

American Institute of Aeronautics and Astronautics

D. Coordinate Systems and Frames of Reference

The VICON motion capture system records the three-dimensional coordinates of moving markers with respect to an inertial coordinate system $(X_I Y_I Z_I)$ (Figure 5), which is set during the calibration process. The origin of the inertial reference frame is set at one of the corners of the capture volume. The X_I and Y_I axes form the horizontal plane and Z_I axis points vertically upwards. At a given instant of time, position of a marker on the butterfly, say T_3, in the inertial frame is identified by its position vector $\mathbf{r}_{T3,I}$. The inertial reference frame is rotated about the Z_I axis to obtain a velocity vector aligned inertial frame $(X_V Y_V Z_V)$ such that the X_V axis is aligned with the projection of the velocity vector, $\mathbf{V}$, onto the horizontal plane.

To describe the motion of the butterfly in a three-dimensional space, we define two additional reference frames: the body and wing reference frames. The body reference frame $(x_b y_b z_b)$ is fixed on and moves with the body, is constructed with successive rotations along the three mutually perpendicular axes of the inertial frame. The origin of the body reference frame is located at the thorax of the butterfly at T_3, which is close to the butterfly center of gravity. The x_b axis is aligned along the longitudinal axis of the body, y_b is directed to the left of the body perpendicular to the x_b axis. The cross product of x_b and y_b axes gives the z_b axis forming a right hand system.

The right wing reference frame $(x_w y_w z_w)$ is constructed with $x_w = RW_4 - RW_2$, y_w pointing to the left, along the vector between RW_3 and T_3. Finally, z_w is obtained by cross product of the x_w and y_w. The inertial, body and wing reference frames follow right hand convention.

The motion and orientation of the butterfly body during flight in three-dimensional space is represented by a 6-DOF system composed of the position in space and three angles. The three orientation angles are the Euler angles, which indicate the rotation of the body about coordinate axes of the inertial frame.
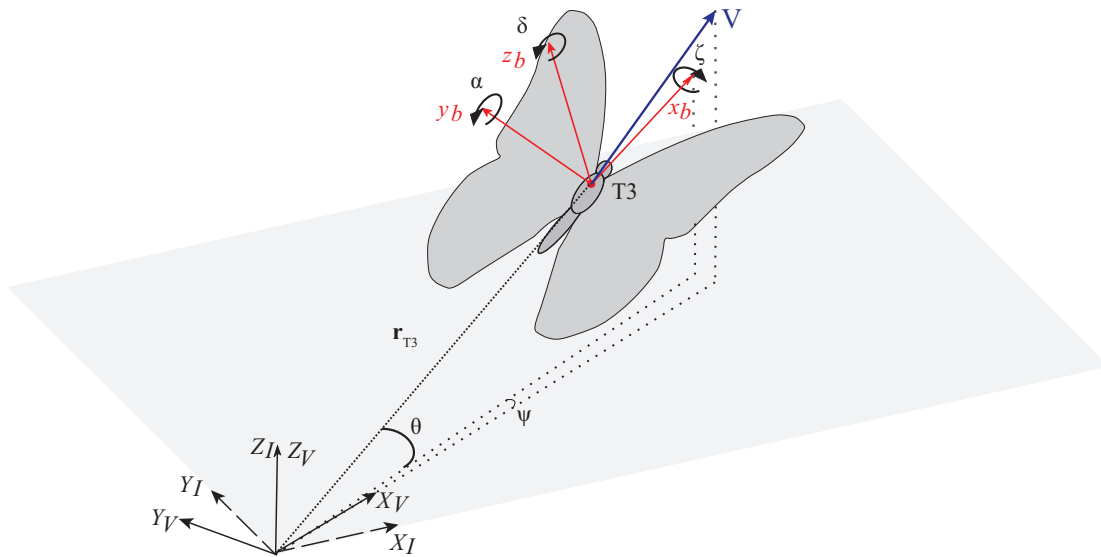

Figure 5. Schematic of the reference frames. A fixed inertial frame and a moving body reference frame.

The thorax markers T_1, T_2 and T_3 are assumed to represent a rigid body. To find the Euler angles of the thorax, it is necessary to find the rotation matrix $R_{I \to b}$ about the origin that transforms the inertial frame of reference to the body frame of reference. The rotation matrix $R_{I \to b}$ can be decomposed into a product of individual elementary rotation matrices around Z_I, Y_I, X_I axes as $R_{I \to b} = R_{Z,I}(\psi) R_{Y,I}(\theta) R_{X,I}(\phi)$, where the rotation matrices are defined as

$$R_{X,I}(\phi) = \begin{pmatrix} \cos\phi & -\sin\phi & 0 \\ \sin\phi & \cos\phi & 0 \\ 0 & 0 & 1 \end{pmatrix}, \quad R_{Y,I}(\theta) = \begin{pmatrix} \cos\theta & 0 & \sin\theta \\ 0 & 1 & 0 \\ -\sin\theta & 0 & \cos\theta \end{pmatrix}, \quad R_{Z,I}(\psi) = \begin{pmatrix} 1 & 0 & 0 \\ 0 & \cos\psi & -\sin\psi \\ 0 & \sin\psi & \cos\psi \end{pmatrix}. \tag{1}$$

where the Euler angles ψ, θ and ϕ are the yaw, pitch and roll angles, respectively, and can be extracted from $R_{I \to b}$ as

American Institute of Aeronautics and Astronautics

$$R_{I \to b} = R_\psi R_\theta R_\phi = \begin{pmatrix} \cos\theta\cos\psi & \cos\psi\sin\phi\sin\theta - \cos\phi\sin\psi & \cos\phi\cos\psi\sin\theta + \sin\phi\sin\psi \\ \cos\theta\sin\psi & \sin\phi\sin\theta\sin\psi + \cos\phi\cos\psi & \cos\phi\sin\theta\sin\psi - \cos\psi\sin\phi \\ \sin\theta & \cos\theta\sin\phi & \cos\phi\cos\theta \end{pmatrix}. \tag{2}$$

The rotation matrix $R_{I \to b}$ is computed using the Singular Value Decomposition (SVD) algorithm. The SVD algorithm computes the optimal rotation in three-dimensional space that transforms one set of points to an another set by minimizing the root mean squared error. The position of thorax markers at a reference time t_0 is taken as the baseline set of points. In order to determine $R_{I \to b}$ at an arbitrary time t, we first find the centroid of the thorax markers T_1, T_2, and T_3, $\mathbf{r}_{\text{centroid}}{}^t$ as

$$\mathbf{r}_{\text{centroid}}{}^t = (\mathbf{r}_{T1} + \mathbf{r}_{T2} + \mathbf{r}_{T3})/3, \tag{3}$$

where the vector components are described in the inertia frame of reference. The translation vector between the current centroid, $\mathbf{r}_{\text{centroid}}{}^t$ and the centroid in the reference configuration, $\mathbf{r}_{\text{centroid}}{}^{t0}$ is simply $\mathbf{r}_{\text{trans}}{}^t = \mathbf{r}_{\text{centroid}}{}^t - \mathbf{r}_{\text{centroid}}{}^{t0}$. In the second step, the optimal rotation matrix $R_{I \to b}$ is computed that transforms the initial configuration to the final configuration after translating the current reference frame to the initial configuration such that both centroid collocate as shown in Figure 6. This process is repeated at each time instant with a new thorax orientation and a fixed reference orientation. As shown in Figure 6(a), the components of T_3 marker in the inertial and body frame is related by

$$\mathbf{r}_{T3,b} = R_{I \to b}(\mathbf{r}_{T3,I} - \mathbf{r}_{\text{trans}}), \tag{4}$$

where the subscript t was omitted for simplicity.

This procedure can be repeated to determine the body-to-wing rotation matrix $R_{b \to w}$. A transformation from inertial reference frame to the wing reference frame is represented by the product of individual rotation matrices as

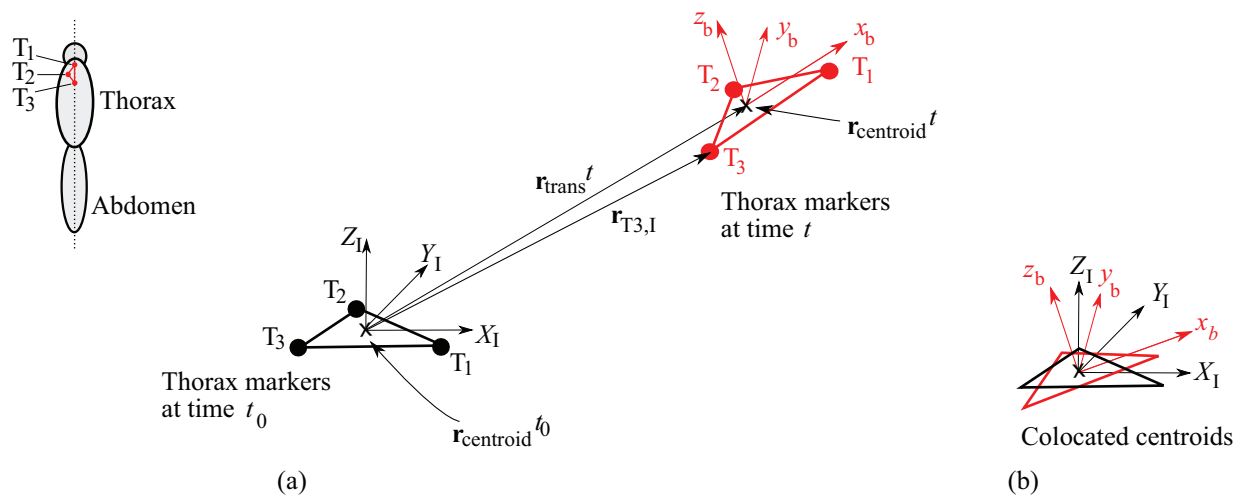$$R_{I \to w} = R_{b \to w} R_{I \to b} \tag{5}$$

Figure 6. Schematic showing the inertial and the body reference frames. A position of a marker in space can be represented in either the inertial frame or the body frame.

9

American Institute of Aeronautics and Astronautics

The butterfly flight involves continuous translation and rotation of the body and wings. By quantifying the wing motion in the body frames of reference, we can eliminate the effects of the body motion on the wings. The flapping motion of the right forewing in the body frame can be expressed in terms of three Euler angles[6]: positional angle, ζ, feathering angle, α, and deviation angle, δ. As shown in Figure 7, clockwise rotation about the longitudinal axis of the body, x_b, is defined as the positional angle ζ. The rotation about the y_b axis is defined as the feathering angle α and rotation about z_b axes is the deviation angle δ. The position of the wing tip at the beginning and end of the downstroke together with the wing root defines the stroke plane[57]. The positional angle at the beginning of the downstroke is denoted by ζ_{max} and at the end of downstroke by ζ_{min}. The stroke amplitude Z is defined as the total sweep angle between the beginning and end of downstroke as $Z=\zeta_{max}-\zeta_{min}$. An average positional angle is $\zeta_a=(\zeta_{max}-\zeta_{min})/2$.

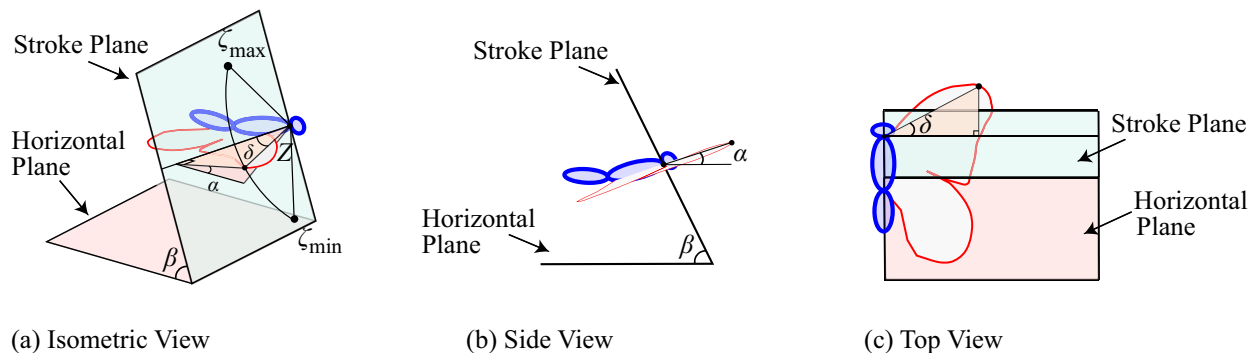(a) Isometric View (b) Side View (c) Top View

Figure 7. Schematic showing the right wing tip at the ends of half stroke together with the wing root forming the stroke plane. The stroke plane angle is denoted by β with the horizontal. Deviation of the wing tip from the stroke plane is denoted by the deviation angle, δ. Feathering angle, θ, is the rotation of the wing surface with respect to the horizontal plane. The stroke amplitude, Z, is defined as the total sweep angle between the beginning and end of downstroke.

Similarly, a stroke plane is defined for wing upstroke by taking the position of the wing tip at the beginning and end of upstroke together with the wing root. The stroke plane orientation with respect to the horizontal is denoted by β. The stroke plane angle, β, not only changes during the up and downstroke, but during different stages of flight. The wing tip normally does not lie on the stroke plane except at the ends of strokes[60]. The deviation of the wing tip from the stroke plane is measured with the deviation angle δ. The feathering angle is also often described as the pitching angle of the wing[6]. It is not an angle of attack as the motion velocity vector of the butterfly also continuously changes its orientation.

III.   Results and Discussion

The methodology and tools developed in Section II are applied on a single butterfly flight to analyze the body and wing kinematics. The results presented here correspond to the Butterfly #1 in Table 1. Statistically significant data and analysis will be reported in the future. Section III.A introduces the trajectory of the climbing flight and the velocity component. This is followed by results from a force balance and lift coefficient in the vertical direction in Section III.B. Section III.C and Section III.D gives a detailed description of the wing and the body kinematics respectively.

A. Trajectory of the Butterfly

The trajectory of the butterfly is the path of the body during flight. Trajectory of the butterfly provides a means to classify a segment of flight into takeoff, climbing or level flight. In our earlier work[54], we observed that the body of the butterfly shows an undulating motion with a significant vertical oscillation during flight. The body oscillation had the same frequency as the flapping motion but with a slight phase shift, suggesting that the body and wing motion are closely coupled. In this study, we provide a more comprehensive and detailed quantification of the body motion. The trajectory is defined with respect to the thorax of the butterfly. The three-dimensional trajectory of a free flying butterfly can be quite complex as illustrated in Figure 8. The butterfly is in a climbing trajectory in Figure

American Institute of Aeronautics and Astronautics

8, where the thorax is ascending at an average rate of 0.75 m/s during two flapping cycles as will be discussed in Section III.B. In addition to climbing, the butterfly can simultaneously vary the orientation of its thorax during flight as shown with a blue line in Figure 8. The projection of the trajectory and the thorax axis on the *x-y* and *y-z* planes show undulating trajectory and a continuously changing thorax orientation.
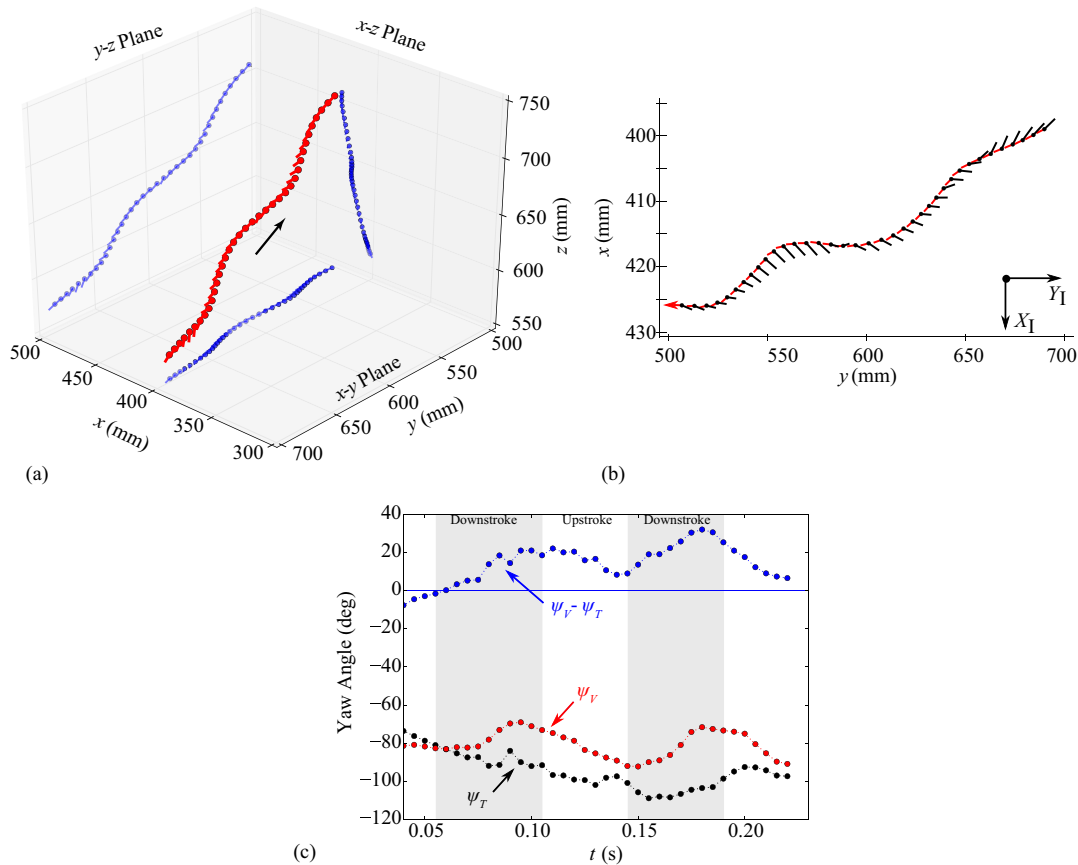

Figure 8. (a) Three-dimensional trajectory of the butterfly in climbing flight. The T_1 marker position is indicated by a red dot every 5 ms. The orientation of the thorax at each frame is shown by a red line. The two-dimensional projections on the coordinate planes are also indicated in blue. (b) The projection of the thorax T_1-T_3 and the local velocity vector on the horizontal plane. T_1 marker is shown as a dot. (c) The yaw angle is defined as the difference of the thorax and the velocity vector projection on the horizontal.

Figure 9(a) shows the position of the T_1 marker during two flapping cycles in the inertial frame. The *x*-component of the T_1 marker in Figure 9(a) shows minimal spatial variation with a change in position of about 0.03 m in two flapping cycles. On the other hand, change in the *y* and the *z* position in the same duration is around 0.19 m and 0.13 m respectively. The undulating oscillations of the thorax is noticeable between up and downstroke motions.

The velocity components of the T_1 marker are shown in Figure 9(b). The velocity components of the T_1 marker shows prominent oscillations when compared to the position. In fact, all three velocity components of the thorax show an increase during downstroke and a decrease during upstroke. The V_x and V_z components are positive whereas V_y is negative. The mean velocity magnitude is 1.28 m/s.
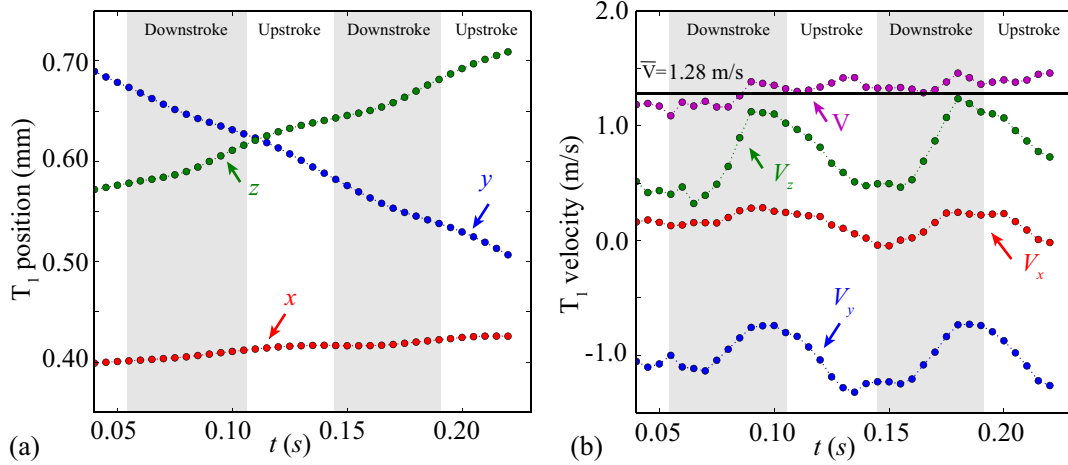
11
American Institute of Aeronautics and Astronautics

Figure 9. (a) Position of T_1 marker in the inertial reference frame. (b) The velocity components of the T_1 marker in the inertial frame. The velocity magnitude, V, and its average are also indicated.

B. Force Balance and Lift Coefficient

Figure 10 shows the trajectory, corresponding variation of the lift coefficient and vertical force during two flapping cycles in a climbing flight. Figure 10(a) clearly depicts two distinct climbing regime. The climb rates are 1.07 m/s and 1.09 m/s in the faster climb regime from the middle of the downstroke to the middle of the upstroke. During the slower climb regime, the rates are 0.44 m/s and 0.52 m/s from the middle of the upstroke to the middle of the downstroke.

The lift coefficient is determined from the force balance on the thorax marker T_1,

$$ma_z = L - mg, \tag{6}$$

where m is the butterfly mass, a_z is the acceleration in vertical direction, L is the lift, and g is the gravitational constant. The acceleration a_z was calculated by numerically differentiating the z position of the T_1 marker (Figure 10 (a)) twice in time. Then the lift coefficient C_L follows as

$$C_L = \frac{L}{\frac{1}{2}\rho V^2 S} = \frac{(a_z + g)}{\frac{1}{2}\rho V^2}\frac{m}{S}, \tag{7}$$

where ρ is the air density, S is the wing area, and V is the speed of the thorax. Since the morphological (Table 1) and motion parameters are known, the instantaneous lift coefficient can be determined as shown in Figure 10(b). A low pass filter is used to remove high frequency oscillations that result from numerical differentiation in velocity and acceleration components.

The ratio between the weight mg and the wing area S is also called the wing loading, an important parameter that characterizes the flight performance. The wing loading for this particular butterfly was 1.61 N/m^2, which is much lower than birds, e.g. Albatross[63]: 140 N/m^2, or man-made aircrafts, e.g. Boeing 747[63]: 7570 N/m^2. Such a low wing loading in general implies a higher maneuverability, lower take-off and landing speeds and higher climb rate. The flight trajectory considered here is a climbing flight where the butterfly climbs 0.12 m in 0.16 s during two flapping cycles, i.e. a climb rate of 0.75 m/s.

Positive lift is generated during the downstroke, whereas the lift is negative during the upstroke with a much lower magnitude as seen in Figure 10(b). The lift coefficient at the beginning of downstroke at t=0.054 s is positive with C_L=3.8. A small drop in C_L observed in the first quarter of the downstroke followed by an increase to a maximum of C_L=10.8 at t=0.085 s. These lift coefficients are much greater than the conventional values on man-made aircraft wings. During downstroke, the wing flaps downward producing positive lift propelling the butterfly upward and forward. As a result, the climb rate increases to 1.07 m/s and 1.09 m/s from the middle of the downstroke until the middle of the upstroke. The magnitude of the lift coefficient at the end of the downstroke at

American Institute of Aeronautics and Astronautics

t=0.105 s is close to zero and turns negative during most of the upstroke with a minimum of C_L=-2.5 near the middle of upstroke at t=0.125 s. The climb rate reduces accordingly to 0.44 m/s and 0.52 m/s for the two upstrokes shown in Figure 10(a). Average lift coefficient for two flapping cycles is found to be 1.93.

The lift force in the vertical direction calculated with Eq. (6) is shown in Figure 10(c). The lift force shown in mN is similar to the C_L curve. The only difference is that the velocity of the thorax, V, continuously varies in time in Eq. (7) as shown in Figure 9(b). The weight of the butterfly with mass m=0.481 g, with markers taken into account is indicated by a red horizontal line. The total weight of the butterfly is W_b=4.71 mN and the averaged vertical force is slightly higher at 5.3 mN when averaged over two motion cycles. The butterfly is able to climb with an average climb rate of 0.75 m/s. During downstroke, the butterfly generates force in the vertical direction and at midstroke, the force exceeds its weight roughly by a factor of six. The net force in the upstroke drops to negative. As a consequence, the climb rate reduces during the upstroke (Figure 10(a)). The climb rate is still positive due to the momentum from the previous downstroke. The climb rate was observed to be higher between the transition from downstroke to upstroke.
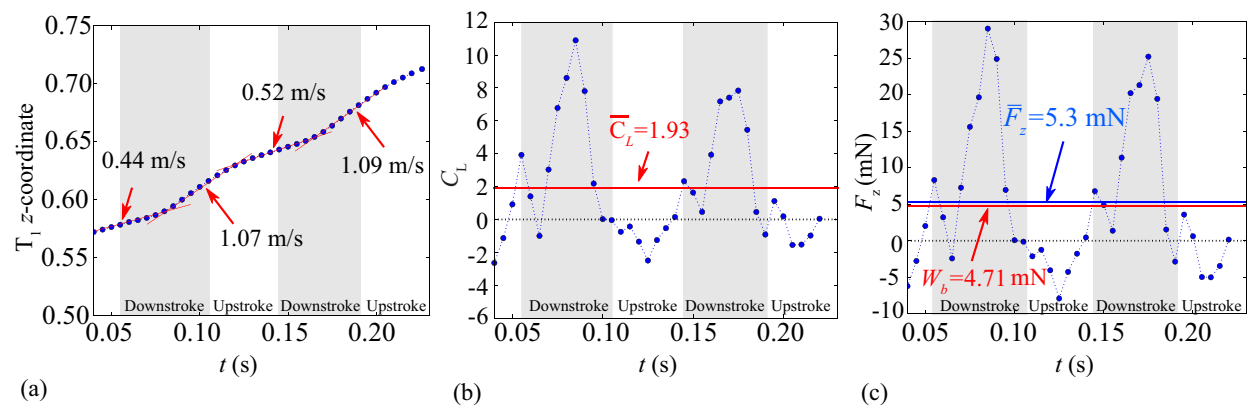

Figure 10. (a) Thorax undulation as shown by the z-coordinate of the T_1 marker in the inertial frame. (b) Lift coefficient C_L calculated using Eq. (7). The red line indicates average lift coefficient in two cycles. (c) The lift force over two flapping cycles calculated from Eq. (6).

C. Flapping Wing Kinematics

Flapping angle, γ, is defined as the angle between the forewings as shown in Figure 11. It is measured by markers at the tip of the left and right forewings, $\mathbf{r}_{LW3}$ and $\mathbf{r}_{RW3}$, respectively in the body reference frame with origin at T_3. In particular, the flapping angle, γ, was calculated as

$$\gamma = \tan^{-1}\left(\frac{|\mathbf{r}_{LW3} \times \mathbf{r}_{RW3}|}{\mathbf{r}_{LW3} \cdot \mathbf{r}_{RW3}}\right). \tag{8}$$

The time history of the flapping angle γ was approximately sinusoidal as shown in Figure 12(a). The amplitude of the flapping motion on an average was found to be around 151 deg.

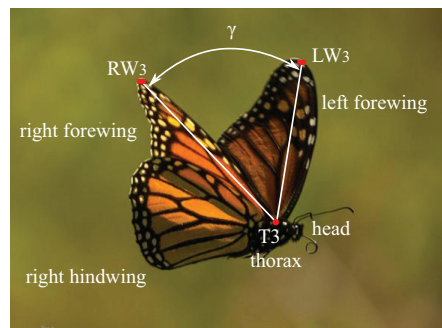**Figure 11. Definition of flapping angle, γ. The leading edge markers on the left and the right fore wings. Adapted from Cranford et al.[54]**

13

Body angles are computed at each time instant. The Euler angles for two flapping cycles are shown in Figure 12(b). The body pitch angle, θ, which is the angle between the thorax and the horizontal plane, varies between $\theta=7$ deg and $\theta=42$ deg. The body pitch shows a periodic oscillation similar to the flapping angle, γ, but with a small phase lag.

At the beginning of the upstroke at $t=0.105$ s, the flapping angle is at its highest with $\gamma=317.7$ deg. The pitch angle of the thorax is close to $\theta=29$ deg at this time instant. The flapping angle decreases during the upstroke as the wings approach each other and the lift coefficient drops causing the butterfly to lose the climb rate. Moreover, the body as a whole is tilted backward, thus increasing the pitch angle. The pitch angle attains a value of around $\theta=33.3$ deg at the mid of upstroke at $t=0.125$ s. During the second half of the upstroke, the thorax tilts forward slightly causing the body pitch angle to drop. By the end of upstroke at $t=0.145$ s, the pitch angle has slightly decreased to $\theta=28.3$ deg. The flapping angle at this point is at its lowest of with $\gamma=23.4$ deg. At the beginning of the downstroke, the body is continuing to tilt forward which decreases the pitch angle further and at the mid of downstroke at $t=0.17$ s, the thorax attains its lowest pitch angle of $\theta=17$ deg. The downward flapping of the wings and the pitch down motion of the thorax takes place simultaneously during the first half of the downstroke. Near the mid of second half of downstroke at $t=0.175$ s, the flapping angle is around $\gamma=203$ deg where the left and the right wings are spread out laterally and the lift generated is at its highest with $C_L=7.8$ (Figure 10(b)). During the second half of the downstroke, the rate of climb increases and thorax simultaneously pitches up and attains $\theta=36.2$ deg at the end of downstroke at $t=0.19$ s.

The yaw angle in Figure 12(b) is defined as the rotation of the thorax about the Z_V axis. The yaw angle varies between $\psi=-8$ deg to $\psi=31$ deg. In general, body orientation is closely related to the type of flight in consideration. Due to the close coupling that exists between body and wing motion, factors such as climb rate (e.g. take-off versus level flight), type of the maneuver (eg. straight versus turning) strongly influence the body orientation angles. Furthermore, to enable comparison between multiple flights while performing a statistical analysis, it is important to eliminate the dependence of body orientation angles on an arbitrarily-fixed inertial reference frame. A definition of angles based on local velocity vector enables a uniform comparison across several individual flights.
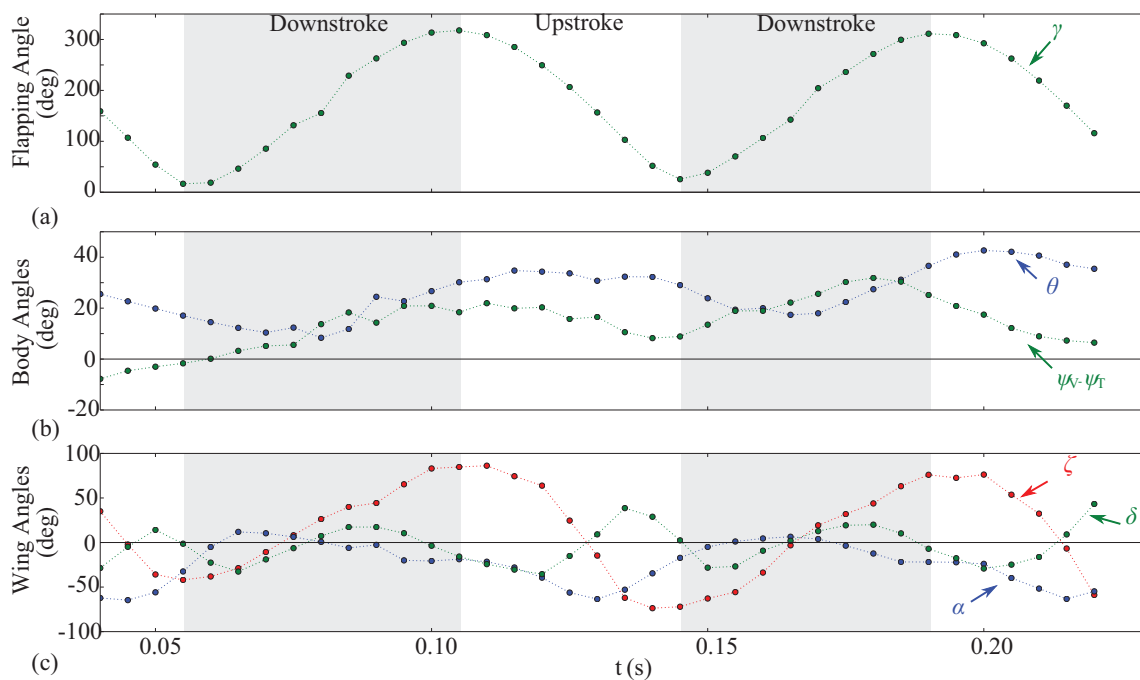

Figure 12. (a) Flapping angle γ. (b) Body pitch and yaw and angles. The yaw angle of the body, $\psi=\psi_V-\psi_T$ is defined in the velocity vector adjusted frame as the rotation about Z_V axis. (c) Wing angles in the body reference frame. Positional angle is denoted by ζ, feathering angle by α and deviation angle by δ.

The wing Euler angles are calculated in the body frame of reference. Positional angle, ζ, has the largest stroke amplitude of Z=151 deg with an average of about ζ_a=76 deg in the two flapping cycles considered in Figure 12(c). The feathering angle, α, was mostly negative during upstroke with a maximum angle of $\alpha \approx$10 deg and a minimum angle of $\alpha \approx$-60 deg recorded during downstroke. In this climbing motion the orientation of the wing chord in the body frame of reference is tilted upwards as depicted in Figure 13. The deviation angle, δ, has a relatively lower magnitude of $\delta \approx$30 deg compared to the positional and feathering angles. The deviation angle, δ, exhibits dual peaks within a full flapping cycle.
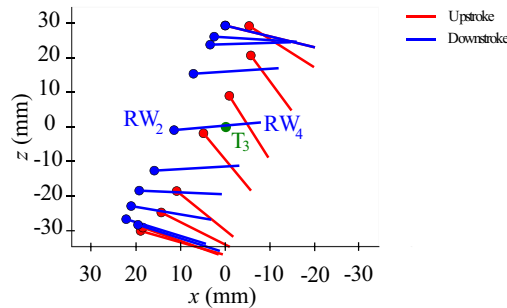

Figure 13. The chord RW$_4$-RW$_2$ in body frame of reference during upstroke and downstroke. The upstroke corresponds to t=0.105 s and t=0.145 s in Figure 12(c). Leading edge, RW$_2$, is shown as a dot. The feathering angle is negative in the clockwise rotation about the y_b axis as seen here during upstroke. During downstroke, the counterclockwise rotation is smaller.

Dominant frequencies of the body and wing angles in Figure 12 are determined with Fast Fourier Transform (FFT). Before performing the FFT, the mean of each time series is calculated and the original data is subtracted from the mean. Figure 14 shows the results from the FFT analysis of the flapping body and wing angles. The flapping angle calculated with left and the right fore wings show a frequency of f=9.52 Hz (Figure 12(a)). Similarly, among the body angles, the body pitch angle appears to have the same frequency as the flapping motion with the yaw and roll angles showing a peak at 4.76 Hz, which is half the frequency of the wings. Among the wing angles, the positional and the feathering angle have a fundamental frequency of 9.52 Hz whereas the deviation angle has a higher frequency of 23.8 Hz, which is 2.5 times greater than the fundamental frequency. The deviation angle, unlike the positional and the feathering angle has two peaks within a halfstroke as seen in Figure 12(c) consistent with the observation in Figure 14(c).
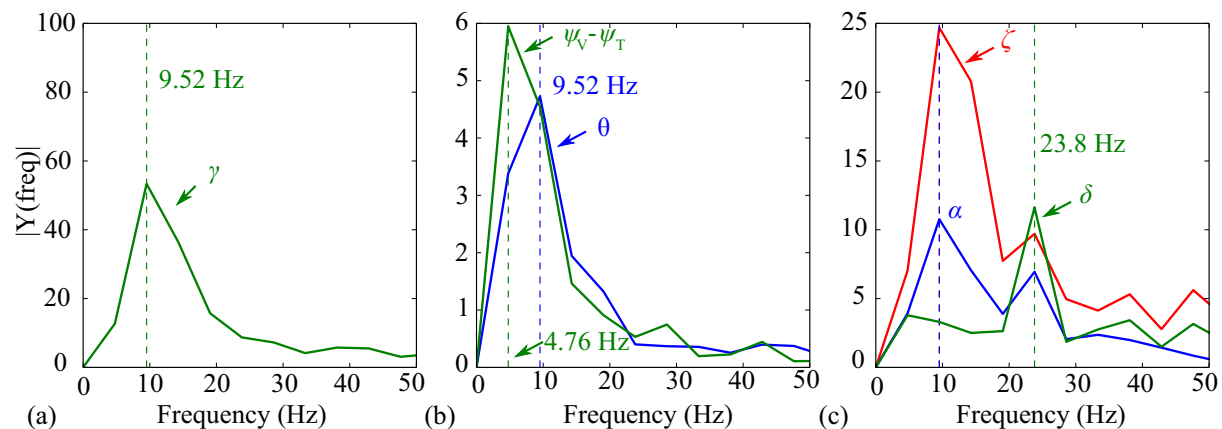

Figure 14. Fast Fourier Transform performed on each of the time series in Figure 12. The flapping frequency is f=9.52 Hz. The body pitch angle shares the same frequency as the flapping angle. Yaw angle has a lower harmonic. Among the wing angles, the positional and the feathering angles have a matching frequency equal to the flapping frequency, f, whereas the deviation angle has a higher frequency than the flapping frequency, consistent with Figure 12(c).

American Institute of Aeronautics and Astronautics

In our earlier study[54], the flapping frequency of Monarch butterflies was observed to be fairly uniform between 9 Hz and 11 Hz, which is close to the frequency found in this study: f=9.52 Hz. In the current study, data is recorded at 200 Hz instead of 100 Hz as in our previous work, improving the accuracy. On the other hand, in the current work we only considered a single flight, whereas in our previous work we reported a statistically significant value from 75 flights. Statistically significant data and analysis of the butterfly flight with the current improved experimental setup will be reported in the future. Similar to our earlier finding that the frequency of the undulating motion of the body was the same as the flapping frequency, current observations indicate that the wing motion and body motion are closely coupled to each other. The body of the butterfly pulls up during the downstroke and undulates with a phase lag with respect to the wing motion as is clearly seen in Figure 1. Most flight dynamics models of flapping wing insects neglect the influence of wing mass and inertia on the body motion[55,64] by assuming that the flapping frequency is much higher than that of body oscillation and that wing mass is much smaller than the body mass. However, for Monarch butterflies, the flapping and body frequencies are similar, and a simplified flight dynamics models cannot be used to analyze the dynamics and stability of butterflies.

The trace of the RW_3 marker in the body frame of reference during a full flapping cycle between t=0.105 s and t=0.19 s is shown in Figure 15. The upstroke position of RW_3 is shown in red and the downstroke in blue. The stroke plane is identified as the plane formed by the T_3 marker in green and the position of RW_3 at the beginning of upstroke and end of upstroke. By definition, the wing tip lies on the stroke plane at the ends of the stroke. It is observed that during upstroke, the wing tip in body frame of reference does not cross the stroke plane and forms a U-shaped trajectory. However, during the downstroke, the wing tip crosses the stroke plane twice: once just after the beginning of the downstroke and once just before the end of the downstroke. The stroke plane makes a β=71.1 deg angle with the horizontal during this stroke. Wing tip markers in the stroke plane reference frame will be reported in the future.
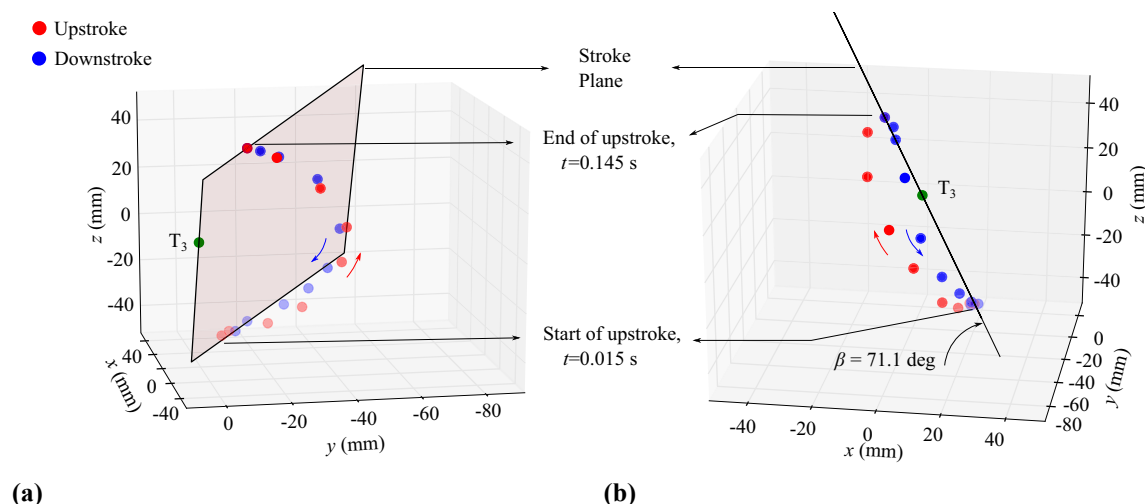

(a)   **(b)**

Figure 15. Position of the right fore wing tip marker RW_3 in the body reference frame during one complete cycle. Red dots indicate upstroke and the blue dots are the position traced during downstroke. (a) Three-dimensional view of the stroke plane drawn by connecting three points: thorax marker T_3, RW_3 at the beginning and end of upstroke. (b) Side view of the stroke plane seen as a line makes β=71.1 deg with the horizontal.

D. Thorax and Abdomen Orientation

The relative orientation of the abdomen with respect to the thorax continuously changes during flight as seen in Figure 1. Furthermore, the body orientation is closely coupled[58] to the wing motion. In an earlier study[54], we reported on the undulating trajectory of the thorax whose frequency closely matched that of the flapping motion with a slight phase lag. In the current study, we measure the individual orientation of the abdomen and the thorax motion by calculating their respective pitch angles with the horizontal.

Figure 16(a) shows the evolution of the pitch angle of the thorax and the abdomen measured with the horizontal. The thorax pitch angle, θ, is calculated as the pitch angle of the longitudinal axis of the thorax represented by markers T_1-T_3. Abdomen pitch angle, χ, is calculated using A_1-A_2 markers as indicated in Figure 3(b). The

American Institute of Aeronautics and Astronautics

difference between the two angles is also shown in Figure 16(a) where a difference angle close to zero indicates that the thorax and the abdomen are aligned. Abdomen, like thorax, shows an undulating motion with positive pitch angle which varies between $\chi=22$ deg and $\chi=56$ deg during two flapping cycles. At the beginning of the upstroke, the thorax and abdomen have nearly the same pitch angle of around $\theta=24$ deg and $\chi=22$ deg at $t=0.105$ s. During the second half of the upstroke, the abdomen angle begins to increase and continues to increase during the following downstroke reaching a peak at the middle of downstroke with $\chi=56$ deg at $t=0.165$ s. During the same interval between $t=0.145$ s and $t=0.165$ s, the thorax shows an opposite trend with decreasing pitch angle with $\theta=16.6$ deg at the middle of downstroke at $t=0.165$ s. The difference between the thorax-abdomen pitch angle is also the highest at the middle of the downstroke. At the middle of the downstroke, the instantaneous lift is also at maximum (Figure 10(b)) and the butterfly has started to climb with the faster climb rate (Figure 10(a)). During the second half of the downstroke, the abdomen pitches down whereas the thorax pitches up and at the end of the downstroke at $t=0.19$ s, both the segments attain an aligned position with $\chi \approx \theta \approx 36.4$ deg. When the thorax and abdomen are aligned, the butterfly is more or less in the faster climb rate regime (Figure 10(a)) with nearly zero or negative lift coefficient (Figure 10(b)).

The markers T_1-T_3 and A_1-A_2 are shown in the YZ plane during the upstroke and downstroke in Figures 16(b) and (c) respectively. The thorax and abdomen are represented as a pair of red and black dashed lines at each frame with direction of climb indicated by an arrow. During upstroke, the relative orientation of the two segments remains nearly aligned as shown by their corresponding pitch angles. During downstroke, the pitch up of the thorax during the second half is noticeable and this corresponds to the climb rate of 1.09 m/s shown in Figure 10(a).

The above observations correspond to a single climbing flight. A more comprehensive description of the body orientation and its possible relation to the climb rate will be reported in the future by considering a statistically significant number of flight segments.
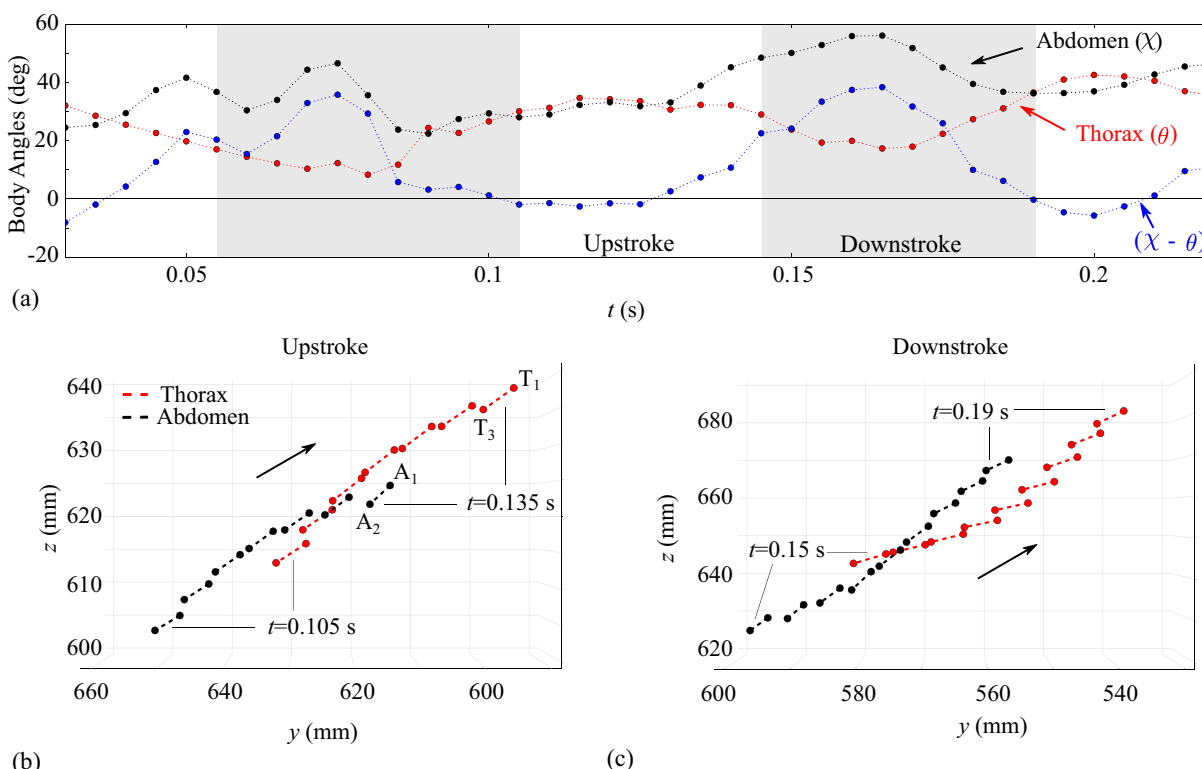

Figure 16. (a) Thorax and abdomen pitch angles and their difference calculated with the horizontal. Thorax orientation represented by markers T_1-T_3 and abdomen orientation represented by markers A_1-A_2 are shown in the YZ plane during (b) Upstroke (c) Downstroke. The arrow indicates the direction of flight.

American Institute of Aeronautics and Astronautics

IV. Concluding Remarks

Body motion and wing kinematics of a free flying Monarch butterfly (*Danaus plexipus*) in climbing trajectory was analyzed using 12 high-resolution motion-tracking cameras in a capture volume of 1.2 m × 1.2 m × 1.5 m. We developed the methodology and the tools needed to quantify the position and orientation of the thorax, abdomen, and wings as well as the instantaneous lift coefficient and climb rate, which can be applied to a large number of flights.

Lift coefficient was calculated using a force balance on the body. Downstroke created a positive C_L with a peak lift coefficient at the middle of downstroke of $C_{L,max}$=10.8. Negative lift coefficient was observed during the upstroke with a smaller magnitude of $C_{L,min}$=-2.5 at the mid of upstroke. As a result of the large lift peak during the downstroke and a relatively smaller minimum upstroke, the butterfly was able to climb with an average rate of 0.75 m/s. Climb rate consistently was higher during the second half of the downstroke until the first half of the upstroke, when compared to climb rate during the other half.

The body and wing orientation angles were calculated with a 6-DOF representation. The abdomen orientation with respect to the thorax changed during a flapping cycle with a pitched down abdomen observed during downstroke. Relative orientation of the abdomen follows an undulating trajectory with higher pitch angles near the first half of the downstroke. The thorax and the abdomen was aligned during the faster regime of the climb, whereas the relative angle between the thorax and the abdomen was at maximum near the middle of the downstroke, coinciding with the maximum C_L and the end of the slower climb regime.

The undulating body pitch angle was found to be closely related to the flapping motion. The positional and feather angles of the right forewing as well as the body pitch angle oscillated with a frequency of 9.52 Hz. The frequency of the wing deviation angle was 2.5 times the flapping frequency, whereas the frequency of the yaw angle of the body was half. The flapping angle of the fore wings was nearly sinusoidal with an amplitude of γ=151 deg. The stroke plane during a flapping cycle was calculated by tracing the wing tip marker of the right forewing at the ends of the stroke. The stroke plane orientation was found to be β=71.1 deg with the horizontal.

Although the presented experimental capability and reported results provide a detailed quantification of the Monarch butterfly motion, we need to place the current results in the context that the current results are based on a single butterfly flight. Main goal of this paper is to present the experimental methodology. Statistically significant analysis of the additional flight tests will be reported in the future along with an analysis of the important physical mechanisms involved in the closely coupled wing-body interaction. For example, the wing motion will be considered in the stroke plane reference frame.

The insights obtained from analysis presented here can be used to identify optimum flight parameters as well as provide an understanding of how butterflies use synchronized body-wing motion control their trajectory.

References

[1]Shyy, W., Aono, H., Chimakurthi, S. K., Trizila, P., Kang, C., Cesnik, C. E. S., and Liu, H., "Recent Progress in Flapping Wing Aerodynamics and Aeroelasticity," *Progress in Aerospace Sciences*, Vol. 46, No. 7, 2010, pp. 284–327.

[2]Rizzetta, D. P., and Visbal, M. R., "Exploration of Plasma-based Control for Low-Reynolds Number Airfoil/gust Interaction," *International Journal of Computational Fluid Dynamics*, Vol. 25, 2011, pp. 509–533.

[3]Keennon, M., Klingebiel, K., Won, H., and Andriukov, A., "Development of the Nano Hummingbird: A Tailless Flapping Wing Micro Air Vehicle," *AIAA-2012-0588*, 50th AIAA Aerospace Sciences Meeting, 09 - 12 January 2012, Nashville, Tennessee, 2012.

[4]Lentink, D., "Biomimetics: Flying Like a Fly," *Nature*, Vol. 498, No. 7454, 2013, pp. 306–307.

[5]Ma, K. Y., Chirarattananon, P., Fuller, S. B., and Wood, R. J., "Controlled Flight of a Biologically Inspired, Insect-Scale Robot," *Science*, Vol. 340, No. 6132, 2013, pp. 603–607.

[6]Shyy, W., Aono, H., Kang, C., and Liu, H., *An Introduction to Flapping Wing Aerodynamics*, Cambridge University Press, New York, New York, 2013.

[7]Magnan, A., *Le vol des insectes*, Hermann, Paris, 1934.

[8]Weis-fogh, T., "Quick Estimates of Flight Fitness in Hovering Animals, Including Novel Mechanisms for Lift Production," *Journal of Experimental Biology*, Vol. 59, No. 1, 1973, pp. 169–230.

[9]Ellington, C. P., van den Berg, C., Willmott, A. P., and Thomas, A. L. R., "Leading-edge Vortices in Insect Flight," *Nature*, Vol. 384, No. 6610, 1996, pp. 626–630.

[10]Dickinson, M. H., Lehmann, F.-O., and Sane, S. P., "Wing Rotation and the Aerodynamic Basis of Insect Flight," *Science*, Vol. 284, No. 5422, 1999, pp. 1954–1960.

[11]Birch, J. M., and Dickinson, M. H., "The Influence of Wing-wake Interactions on the Production of Aerodynamic Forces in Flapping Flight," *Journal of Experimental Biology*, Vol. 206, No. 13, 2003, pp. 2257–2272.

[12]Sane, S. P., and Dickinson, M. H., "The Aerodynamic Effects of Wing Rotation and a Revised Quasi-Steady Model of Flapping Flight," *Journal of Experimental Biology*, Vol. 205, No. 8, 2002, pp. 1087–1096.

[13]Vogel, S., *Comparative Biomechanics*, Life's Phy ed., Princeton University Press, New Jersey, 2013.

[14]Srygley, R. B., and Thomas, A. L. R., "Unconventional Lift-generating Mechanisms in Free-Flying Butterflies.," *Nature*, Vol. 420, No. 6916, 2002, pp. 660–4.

[15]Muijres, F. T., Elzinga, M. J., Melis, J. M., and Dickinson, M. H., "Flies Evade Looming Targets by Executing Rapid Visually Directed Banked Turns," *Science*, Vol. 344, No. 6180, 2014, pp. 172–177.

[16]Dillon, M. E., and Dudley, R., "Surpassing Mt. Everest: Extreme Flight Performance of Alpine Bumble-bees.," *Biology letters*, Vol. 10, 2014, p. 20130922.

[17]Mountcastle, A. M., and Combes, S. A., "Wing Flexibility Enhances Load-Lifting Capacity in Bumblebees," *Proceedings of the Royal Society B: Biological Sciences*, Vol. 280, No. 1759, 2013, pp. 20130531–20130531.

[18]Wang, Z. J., "Dissecting Insect Flight," *Annual Review of Fluid Mechanics*, Vol. 37, No. 1, 2005, pp. 183–210.

[19]Jongerius, S. R., and Lentink, D., "Structural Analysis of a Dragonfly Wing," *Experimental Mechanics*, Vol. 50, No. 9, 2010, pp. 1323–1334.

[20]Wang, Z. J., and Russell, R. D., "Effect of Forewind and Hindwing Interactions on Aerodynamic Forces and Power in Hovering Dragonfliy Flight," *Physical Review Letters*, Vol. 99, 2007, p. 148101.

[21]Alexander, D. E., "Unusual Phase Relationships Between the Forewing and Hindwings in Flying Dragonflies," *Journal of Experimental Biology*, Vol. 109, 1984, pp. 379–383.

[22]Wang, J. K., and Sun, M., "A Computational Study of the Aerodynamics and Forewing-hindwing Interaction of a Model Dragonfly in Forward Flight," *Journal of Experimental Biology*, Vol. 208, No. 19, 2005, pp. 3785–3804.

[23]Dudley, R., "Biomechanics of Flight in Neotropical Butterflies: Aerodynamics and Mechanical Power Requirements," *Journal of experimental biology*, Vol. 357, No. 1, 1991, pp. 335–357.

[24]Thomas, A. L. R., Taylor, G. K., Srygley, R. B., Nudds, R. L., and Bomphrey, R. J., "Dragonfly Flight: Free-Flight and Tethered Flow Visualizations Reveal a Diverse Array of Unsteady Lift-generating Mechanisms, Controlled Primarily via Angle of Attack," *Journal of Experimental Biology*, Vol. 207, No. 24, 2004, pp. 4299–4323.

[25]Srygley, R. B., "Locomotor Mimicry in Butterflies? The Associations of Positions of Centres of Mass among Groups of Mimetic, Unprofitable Prey," *Philosophical Transactions of the Royal Society of London B: Biological Sciences*, Vol. 343, No. 1304, 1994, pp. 145–155.

[26]Dudley, R., and Srygley, R., "Flight Physiology of Neotropical Butterflies: Allometry of Airspeeds During Natural Free Flight," *The Journal of experimental biology*, Vol. 191, No. 1, 1994, pp. 125–39.

[27]Lin, T., Zheng, L., Hedrick, T., and Mittal, R., "The Significance of Moment-of-inertia Variation in Flight Manoeuvres of Butterflies," *Bioinspiration & Biomimetics*, Vol. 7, No. 4, 2012, p. 044002.

[28]Carpenter, G. D. H., "Further Evidence that Birds do Attack and Eat Butterflies," *Proceedings Zoology Society London A*, 1937, pp. 223–247.

[29]Dudley, R., *The Biomechanics of Insect Flight: Form, Function, Evolution*, Princeton University Press, New Jersey, 2002.

[30]Srygley, R. B., and Dudley, R., "Correlations of the Position of Center of Body Mass With Butterfly Escape Tactics," *The Journal of Experimental Biology*, Vol. 174, 1993, pp. 155–166.

[31]Brower, L., "Monarch Butterfly Orientation: Missing Pieces of a Magnificent puzzle," *The Journal of experimental biology*, Vol. 199, 1996, pp. 93–103.

[32]Masters, A. R., Malcolm, S. B., and Brower, L. P., "Monarch Butterfly (Danaus Plexippus) Thermoregulatory Behavior and Adaptations for Overwintering in Mexico," *Ecology*, Vol. 69, No. 2, 1988, p. 458.

[33]Merlin, C., Gegear, R. J., and Reppert, S. M., "Antennal Circadian Clocks Coordinate Sun Compass Orientation in Migratory Monarch Butterflies," *Science*, Vol. 325, No. 5948, 2009, pp. 1700–1704.

[34]Brower, L. P., Fink, L. S., and Walford, P., "Fueling the Fall Migration of the Monarch Butterfly," *Integrative and Comparative Biology*, Vol. 46, No. 6, 2006, pp. 1123–1142.

[35]Slayback, D. a., Brower, L. P., Ramirez, M. I., and Fink, L. S., "Establishing the Presence and Absence of Overwintering Colonies of the Monarch Butterfly in Mexico by the Use of Small Aircraft," *American Entomologist*, Vol. 53, No. 1, 2007, pp. 28–40.

[36]Gibo, D. L., "Altitudes Attained By Migrating Monarch Butterflies, Danaus P. Plexippus (Lepidoptera: Danainae), as Reported By Glider Pilots," *Canadian Journal of Zoology*, Vol. 59, 1981, pp. 571–572.

[37]Taylor, L. R., "Insect Migration, Flight Periodicity and the Boundary Layer," *The Journal of Animal Ecology*, Vol. 43, No. 1, 1974, p. 225.

[38]Gibo, D. L., and Pallett, M. J., "Soaring Flight of Monarch Butterflies, *Danaus plexippus* (Lepidoptera: Danaidae), during the late summer migration in southern Ontario," *Canadian Journal of Zoology*, Vol. 57, No. 7, 1979, pp. 1393–1401.

[39]Kovac, M., Vogt, D., Ithier, D., Smith, M., and Wood, R., "Aerodynamic Evaluation of Four Butterfly Species for the Design of Flapping-gliding Robotic Insects," *IEEE International Conference on Intelligent Robots and Systems*, 2012, pp. 1102–1109.

[40]Paoletti, P., and Mahadevan, L., "Intermittent Locomotion as an Optimal Control Strategy," *Proceedings of the Royal Society A: Mathematical, Physical and Engineering Sciences*, Vol. 470, No. 2164, 2014, pp. 20130535–20130535.

[41]Guerra, P. A., Gegear, R. J., and Reppert, S. M., "A Magnetic Compass Aids Monarch Butterfly Migration," *Nature Communications*, Vol. 5, No. May, 2014, p. 4164.

[42]Dudley, R., and Ellington, C. P., "Mechanics of Forward Flight in Bumblebees I. Kinematics and Morphology," *Journal of Experimental Biology*, Vol. 52, 1990, pp. 19–52.

[43]Scoble, M. J., *The Lepidoptera*, Oxford University Press, New York, 1992.

[44]Betts, C. R., and Wootton, R. J., "Wing Shape and Flight Behaviour in Butterflies (Lepidoptera: Papilionoidea and Hesperioidea): A Preliminary Analysis," *Journal of Experimental Biology*, Vol. 138, No. 1, 1988, pp. 271–288.

[45]Tanaka, H., and Shimoyama, I., "Forward Flight of Swallowtail Butterfly with Simple Flapping Motion.," *Bioinspiration & biomimetics*, Vol. 5, No. 2, 2010, p. 026003.

[46]Steppan, S., "Flexural Stiffness Patterns of Butterfly Wings (Papilionoidea)," *J. Res. Lepid*, Vol. 1996, No. May 1998, 1996, pp. 61–77.

[47]Tanaka, H., Whitney, J. P., and Wood, R. J., "Effect of Flexural and Torsional Wing Flexibility on Lift Generation in Hoverfly Flight.," *Integrative and comparative biology*, Vol. 51, No. 1, 2011, pp. 142–50.

[48]Willmott, A. P., and Ellington, C. P., "The Mechanics of Flight in the Hawkmoth Manduca Sexta," *Journal of Experimental Biology*, Vol. 2722, 1997, pp. 2705–2722.

[49]Ristroph, L., Berman, G. J., Bergou, A. J., Wang, Z. J., and Cohen, I., "Automated Hull Reconstruction Motion Tracking (HRMT) Applied to Sideways Maneuvers of Free-flying Insects.," *The Journal of experimental biology*, Vol. 212, 2009, pp. 1324–1335.

[50]Walker, S. M., Thomas, A. L. R., and Taylor, G. K., "Photogrammetric reconstruction of high-resolution surface topographies and deformable wing kinematics of tethered locusts and free-flying hoverflies.," *Journal of the Royal Society Interface*, Vol. 6, No. 33, 2009, pp. 351–66.

[51]Zheng, L., Hedrick, T. L., and Mittal, R., "Time-varying Wing-twist Improves Aerodynamic Efficiency of Forward Flight in Butterflies.," *PloS one*, Vol. 8, No. 1, 2013, p. e53060.

[52]Zheng, L., Wang, X., Khan, A., Vallance, R., and Mittal, R., "A Combined Experimental-Numerical Study of the Role of Wing Flexibility in Insect Flight," *AIAA 2009-382*, 47th AIAA Aerospace Science Meeting, 5 - 8 January 2009, Orlando, Florida, 2009.

[53]Koehler, C., Liang, Z., Gaston, Z., Wan, H., and Dong, H., "3D Reconstruction and Analysis of Wing Deformation in Free-Flying Dragonflies.," *The Journal of experimental biology*, Vol. 215, No. Pt 17, 2012, pp. 3018–27.

[54]Cranford, J., Kang, C., Landrum, D. B., and Slegers, N., "Experimental Characterization of Butterfly in Climbing Flight," *AIAA Aviation*, Dallas, TX, 22-26 June 2015, 2015, pp. AIAA–2015–2328.

[55]Sun, M., "Insect flight dynamics: Stability and Control," *Reviews of Modern Physics*, Vol. 86, No. 2, 2014, pp. 615–646.

[56]Kim, E. J., Wolf, M., Ortega-Jimenez, V. M., Cheng, S. H., and Dudley, R., "Hovering Performance of Anna's hummingbirds (*Calypte anna*) in Ground Effect," *Journal of The Royal Society Interface*, Vol. 11, No. 98, 2014, pp. 20140505–20140505.

[57]Dudley, R., "Biomechanics of Flight in Neotropical Butterflies: Morphometrics and Kinematics," *Journal of Experimental Biology*, Vol. 150, 1990, pp. 37–53.

[58]Sunada, S., and Kawachi, K., "Performance of a Butterfly in Take-Off Flight," *Journal of experimental Biology*, Vol. 277, No. 183, 1993, pp. 249–277.

[59]Fei, Y.-H. J., and Yang, J.-T., "Importance of Body Rotation During the Flight of a Butterfly," *Physical Review E*, Vol. 93, No. 3, 2016, p. 033124.

[60]Ellington, C. P., "The Aerodynamics of Hovering Insect Flight. III. Kinematics," *Philosophical Transactions of the Royal Society B: Biological Sciences*, Vol. 305, No. 1122, 1984, pp. 41–78.

[61]Vicon Motion Systems, *Vicon Nexus 1 Manual*, 2014.

[62]Alonso-Mejía, A., Rendon-Salinas, E., Montesinos-Patiño, E., and Brower, L. P., "Use of Lipid Reserves by Monarch Butterflies Overwintering in Mexico: Implications for Conservation," *Ecological Applications*, Vol. 7, No. 3, 1997, pp. 934–947.

[63]Tennekes, H., *The Simple Science of Flight: From Insects to Jumbo Jets*, 2009.

[64]Orlowski, C. T., and Girard, A. R., "Modeling and Simulation of Nonlinear Dynamics of Flapping Wing Micro Air Vehicles," *AIAA Journal*, Vol. 49, No. 5, 2011, pp. 969–981.

[65]Combes, S. A., and Daniel, T. L., "Flexural Stiffness in Insect Wings II. Spatial Distribution and Dynamic Wing Bending," *Journal of Experimental Biology*, Vol. 206, No. 17, 2003, pp. 2989–2997.

[66]Wootton, R. J., "Leading Edge Section and Asymmetric Twisting in the Wings of Flying Butterflies," *Journal of Experimental Biology*, Vol. 180, 1993, pp. 105–117.

[67]Nakata, T., and Liu, H., "Aerodynamic Performance of a Hovering Hawkmoth with Flexible Wings: A Computational Approach," *Proceedings of the Royal Society B: Biological Sciences*, Vol. 279, No. 1729, 2012, pp. 722–731.

American Institute of Aeronautics and Astronautics